

Electron-electron and electron-phonon collision cross sections in CsV₃Sb₅

Charles Menil,¹ Andrea Capa Salinas,² Stephen D. Wilson,² Benoît Fauqué,¹ and Kamran Behnia¹

¹*Laboratoire de Physique et d'Étude de Matériaux (CNRS)
ESPCI Paris, PSL Research University, 75005 Paris, France*

²*Materials Department, University of California
Santa Barbara, California 93106, USA*

(Dated: February 24, 2026)

AV₃Sb₅ (A = K, Rb, Cs) are kagome metals and superconductors, attracting much recent attention as nexus of multiple quantum states. Here, through a systematic study of electric and thermal transport of CsV₃Sb₅, we identify it as a metallic Fermi liquid with moderate electronic correlations and strong electron-phonon (e-ph) collision cross section. We observe contributions to the inelastic electrical resistivity, each dominating within a distinct temperature window. The prefactor of the T² is consistent with the Kadowaki-Woods scaling for a Fermi liquid with moderate correlation. By performing thermal conductivity measurements at zero and finite magnetic field, we separate the electronic and the lattice contributions to the thermal conductivity. The Wiedemann-Franz law is satisfied in the zero-temperature limit, while a downward deviation emerges at finite temperature due to the mismatch between the prefactors of the electrical and thermal quadratic resistivities, as reported in other metals. The Bloch-Grüneisen description of electron-phonon scattering successfully accounts for both electronic thermal and electrical transport, indicating a remarkably large e-ph collision cross section in CsV₃Sb₅.

Discovered in 2019, the AV₃Sb₅ (A=K, Rb, Cs) family are kagome metals with a Charge Density Wave (CDW) instability and a superconducting ground state [1, 2]. They have been a subject of much attention as a platform to explore the interplay between geometric frustration and collective electronic phenomena.

The rich phase diagram of CsV₃Sb₅ has been experimentally mapped [3]. The possible loss of time reversal symmetry in the CDW state despite the absence of any magnetic order [3–12] has been one debated topic. In addition to the CDW, with an onset of ≈ 100 K (the onset of CDW), and superconductivity, with a critical temperature of ≈ 3 K, other anomalies have been reported, notably at ≈ 30 K [13, 14] and ≈ 60 K [15] and a nematic state has also been invoked [16].

Thanks to studies of quantum oscillations [17–22], the Fermi surface of this metal is fairly well documented. The reconstruction of the Fermi surface by the CDW [17], generates numerous detectable frequencies. Despite its layered structure, this metal hosts three-dimensional pockets [18]. Pressure destroys the CDW and the Fermi surface reconstruction. A study of quantum oscillations under pressure has explored the non-reconstructed Fermi surface [22] and found it in agreement with DFT expectations.

Despite the wealth of information gathered by these studies, a number of basic questions have not been explicitly answered. Does the electronic transport in this metal correspond to what is expected in a Fermi liquid? If yes, what is the amplitude of electron-electron scattering and how does it compare to other metallic Fermi liquids? What about electron-phonon scattering? What is the share of electronic and phononic contributions to the total thermal conductivity? Is

there any sign of electron-electron scattering in thermal channel? What is the effect of phonon scattering on the electronic thermal conductivity compared to other metals?

Previous studies of transport in CsV₃Sb₅ [13, 14, 23–25] focused on possible signatures of nematicity and symmetry breaking, not on these questions. Here, we address them by reporting on a study electric and thermal transport focused on separating different contributions to the electric and thermal transport below 35 K. According to our findings, CsV₃Sb₅ is a Fermi liquid with electronic correlations of moderate strength. On the other hand, it has a remarkably large electron-phonon collision cross section, presumably due to the vicinity of a structural transition. We quantify the respective share of scattering by electrons and phonons to the electric conductivity and to the electronic component of the thermal conductivity. We also separates the electronic and the phononic contributions to heat transport. The former obeys the Wiedemann-Franz law in the zero-temperature limit but deviates downward at finite temperature. The latter implies a phonon mean-free-path well below the sample size. Thus, according to our study, the standard picture of solid-state transport gives a reasonable account of in-plane electric and thermal resistivity in this solid. It provides quantitative numbers to be confronted with what, at least in principle, can be computed from the specific electronic and structural properties of this metal.

The in-plane electrical resistivity, ρ , of a CsV₃Sb₅ single crystal measured by a four-electrode method, is shown in Figure 1a. At zero-field, the superconducting transition is visible at ≈ 3 K. Upon the application of a magnetic field of 1 T, perpendicular to the

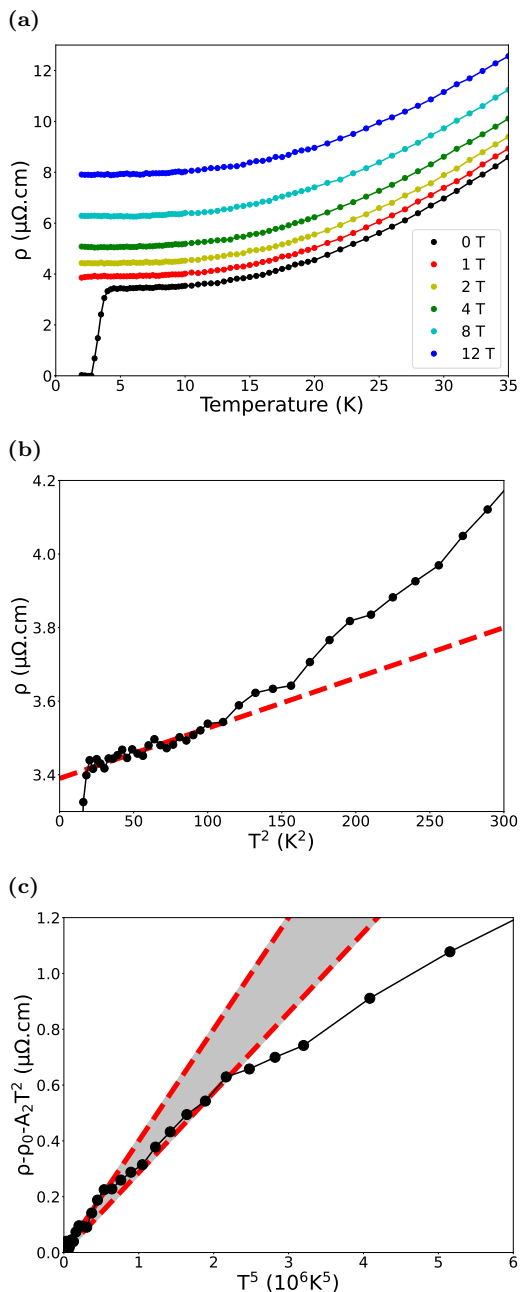


Figure 1: Low Temperatures electrical resistivity of CsV_3Sb_5 . (a) Resistivity from 2 K to 35 K for several applied magnetic fields along crystal c -axis. (b) Resistivity at zero magnetic field versus temperature square. The red line shows T -square resistivity for temperatures between 4 K and 10 K. (c) Residual resistivity at zero magnetic field versus temperature to the power 5. The red lines show estimated minimum and maximum T^5 resistivity. The gray area shows the incertitude on the T^5 resistivity.

kagome planes, the superconducting transition disappears. Resistivity curves shift vertically and almost rigidly with magnetic field.

Figure 1b is a plot of zero-field resistivity as function of the square of temperature. One can see that between the superconducting transition and ≈ 10 K, ρ is linear in T^2 . A linear fit in this narrow window

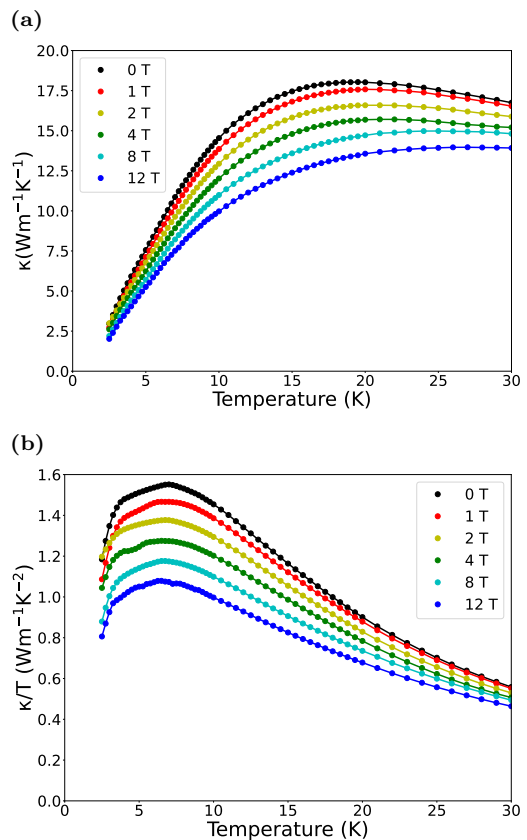


Figure 2: Thermal conductivity of CsV_3Sb_5 crystal. (a) Thermal conductivity from 2 K to 30 K for several applied magnetic fields along crystal c -axis. (b) Thermal conductivity divided by temperature, from 2 K to 30 K. Resistivity and thermal conductivity have been measured on the same sample.

yields a finite intercept at $T=0$: ρ_0 . At high temperature, the data deviates upward from this linear fit. This deviation signals the presence of a larger exponent for inelastic resistivity at higher temperatures. The most plausible candidate is a T^5 dependence, expected by the Bloch-Grüneisen law of electron-phonon scattering when $T \ll \Theta_D$. This hypothesis is confirmed in Fig. 1c. It is a plot of resistivity, after the subtraction of its constant (ρ_0) and quadratic (A_2T^2) terms, as function of T^5 . Below 18 K, one can detect a T^5 , with an uncertainty on the slope, which is highlighted by the shaded area. Note the downward deviation at higher temperatures, signaling evolution towards a lower exponent. This conforms to the Bloch-Grüneisen picture, where the exponent is expected to gradually evolve towards 1, as the Debye temperature ($\Theta_D \approx 160$ K [26]) is approached.

Thus, we conclude that below 18 K (that is, $\approx \Theta_D/10$), ρ , follows:

$$\rho = \rho_0 + A_2T^2 + A_5T^5 \quad (1)$$

Here, ρ_0 is the residual resistivity, A_2 is the T -square

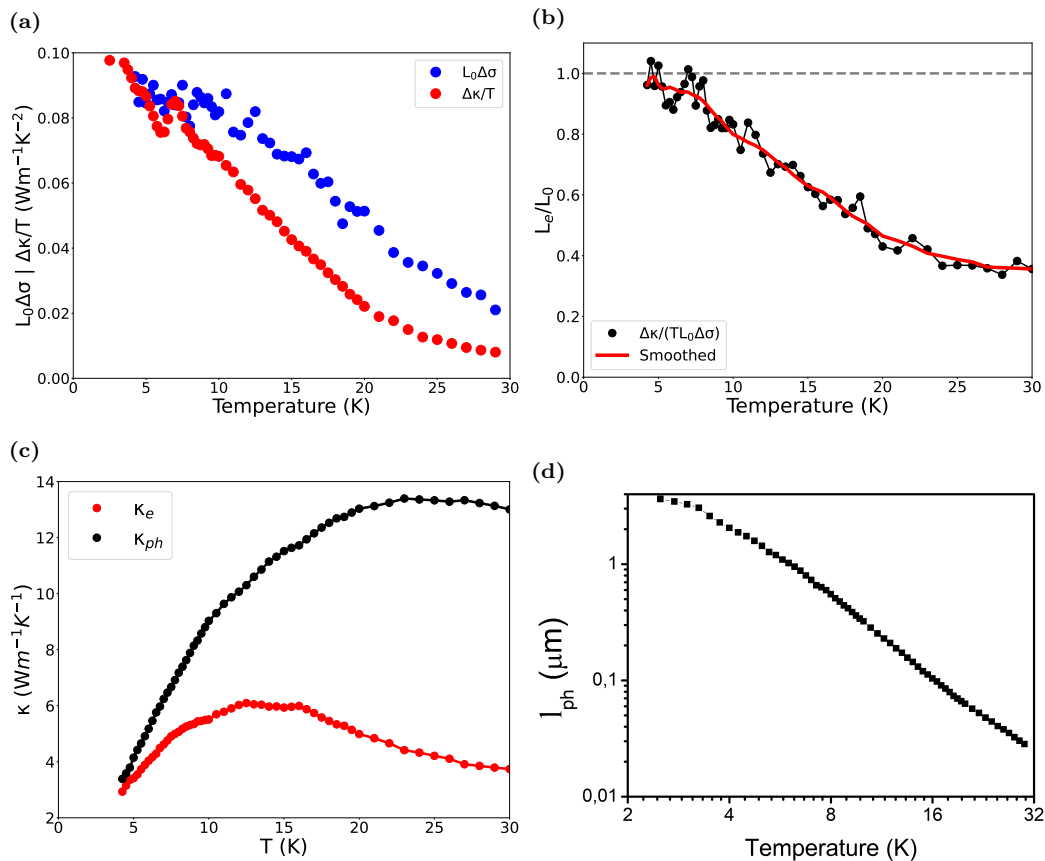


Figure 3: Separation between electrons and phonon contribution in thermal conductivity. (a) Difference in electronic and thermal conductivity between measurements under 0 T and 1 T. (b) L divided by L_0 obtained from measurements at 0 T and 1 T. (c) Phononic and electronic thermal conductivity under zero magnetic field. (d) The phonon mean free path, l_{ph} vs. temperature, in a log-log scale. It has been calculated using the kinetic formula $\kappa = \frac{1}{3}Cv_sl_{ph}$, the reported sound velocity ($v_s = 1960 \text{ m.s}^{-1}$ [23]) and the experimentally measured heat capacity [26].

prefactor, caused by e-e scattering and A_5 , the T^5 prefactor, due to e-ph scattering.

A fit to our zero-temperature data yields $\rho_0 = 3.4 \mu\Omega.\text{cm}$, $A_2 = 1.24 \pm 0.1 \text{ n}\Omega.\text{cm.K}^{-2}$ and $A_5 = 2.6 \pm 0.2 \times 10^{-7} \mu\Omega.\text{cm.K}^{-5}$. In contrast to the residual resistivity, which is extrinsic and is set by the concentration of defects and impurities, the two other terms are set by the collision cross section of carriers of charge with scattering centers, and therefore intrinsic to the metal in question.

The quadratic term, AT^2 , is ubiquitous in metals, save for exceptions, such as 'strange' [27] or 'polar' [28] ones. It is caused by electron-electron scattering [29–31]. Since the phase space of such collisions is proportional to $(k_B T/E_F)^2$, it is easily observable in dilute [32] or in strongly correlated metals [30], which have both a small Fermi energy E_F , but not in dense and/or weakly correlated metals. The prefactor A_2 , together with the electronic T-linear specific heat (i.e. the Sommerfeld coefficient, γ), allows us to put the system on the Kadowaki–Woods plot [29, 30, 33]. Combined with $\gamma \simeq 20 \text{ mJ.mol}^{-1}.\text{K}^{-2}$ [26, 34], our data yields: $A_2/\gamma^2 \simeq 3 \times 10^{-6} \mu\Omega.\text{cm. mJ}^{-1}.\text{mol}$ in

CsV_3Sb_5 . This value is three times lower than the Kadowaki-Woods ratio for strongly correlated metals $A_2/\gamma^2[KW] = 10^5 \mu\Omega.\text{cm. mJ}^{-1}.\text{mol}$ [30], but eight times larger than the Rice ratio for weakly correlated metals $A_2/\gamma^2[Rice] = 0.4 \times 10^{-6} \mu\Omega.\text{cm.mJ}^{-1}.\text{mol}$ [29]. Thus, like many other Fermi liquids, lying between these two fuzzy boundaries, CsV_3Sb_5 is a moderately correlated Fermi liquid [33].

As for electron-phonon scattering, it is noteworthy that the amplitude of A_5 prefactor in CsV_3Sb_5 is large. In gold, with a comparable Debye temperature, Θ_D , the tabulated resistivity data [35] yields a fifty times smaller T^5 prefactor ($A_5(Au) \simeq 4 \times 10^{-9} \mu\Omega.\text{cm.K}^{-5}$). The unusually narrow window of T-square resistivity is connected to this feature. A relatively small T^2 term together with a relatively large amplitude of the T^5 term, confine the former to below 10 K.

Let us now turn our attention to thermal transport. We measured the thermal conductivity (κ) of the same CsV_3Sb_5 sample using a one-heater-two-thermometers method using the same electrodes as for measurements of the electric resistivity. Figure

2 displays the thermal conductivity, κ , in zero and finite magnetic field. In the whole range of temperature (from 2 K to 30 K) and magnetic field ($B \leq 12$ T), the amplitude of κ is steadily diminished with increasing field. Our data is consistent with two other previous reports [26, 36] (See the supplement for a discussion of consistency between different data sets).

Phonons and mobile electrons can both carry heat. In order to separate the phononic, κ_{ph} , and the electronic, κ_e , components of κ , one can exploit the fact that, because of the electronic magnetoresistance, κ_e is significantly affected by the magnetic field. In contrast, κ_{ph} has no field dependence (at least, not a significant one). Such a procedure of using a magnetic field to separate κ_{ph} and κ_e has been used in semimetals [37–41] as well as in metallic oxides [42, 43].

Specifically, we are interested to know the amplitude and the temperature dependence of the electronic Lorenz number, defined as $L_e = \frac{\kappa_e}{T\sigma}$. Let us assume that magnetic field affects κ and σ in a similar way. In other words, at a given temperature, L_e is independent of magnetic field. This is a reasonable assumption provided that we limit ourselves to small magnetic fields. This assumption allows us to quantify L_e experimentally by measuring $\Delta\kappa$ and $\Delta\sigma$, the field-induced variation of thermal and electrical conductivities and deducing $L_e = \frac{\Delta\kappa}{T\Delta\sigma}$. These assumptions lead to the following expression for κ_e :

$$\kappa_e = \sigma \frac{\Delta\kappa}{\Delta\sigma} \quad (2)$$

Afterwards, the phononic component can be obtained by a simple subtraction: $\kappa_{ph} = \kappa - \kappa_e$.

The results are depicted in Figure 3. Let us first consider the fate of the Wiedemann-Franz (WF) law, according to which, in the zero temperature limit, $L_e = L_0$ ($L_0 = \frac{\pi^2}{3} \left(\frac{k_B}{e}\right)^2$ is the so-called Sommerfeld value). Figure 3a is a plot comparing the amplitude and temperature dependence of $\Delta\kappa/T$ and $L_0\Delta\sigma$, where $\Delta\kappa = \kappa(0T) - \kappa(1T)$ and $\Delta\sigma = \sigma(0T) - \sigma(1T)$. Between 4 K and 7 K, the two curves are close to each other as expected by the WF law. Figure 3b, which is a plot of the temperature dependence of L_e/L_0 is more explicit. Below 7 K, Wiedemann-Franz law is respected within experimental resolution. A downward departure is clearly visible. Such a deviation was previously observed in other metals, both strongly correlated such as CeRhIn₅ [44] and UPt₃ [45] or in weakly correlated ones, such as W [46] and WP₂ [47].

Having quantified L_e , we can separate the electronic and the lattice components of the thermal conductivity. κ_{ph} and κ_e are plotted in Figure 3c. In the whole temperature range, κ_{ph} is larger than κ_e . In the kinetic theory of gases [48], an expression links κ_{ph} to the phonon mean free path, l_{ph} : $\kappa_{ph} = \frac{1}{3}C_{ph}v_{ph}l_{ph}$.

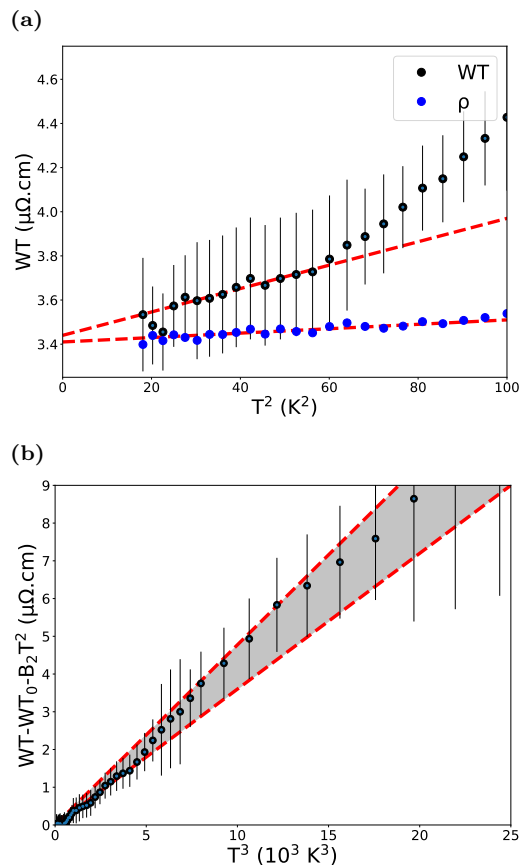


Figure 4: Electrical thermal conductivity (WT). (a) WT at 0 T. (a) WT and ρ versus temperature square. Red lines show T-square resistivity, for temperatures up to 7 K for WT and 10 K for ρ . (b) WT without the constant and the quadratic term as function of temperature cube. The red lines show estimated maximum and minimum T-cube dependence for temperatures. The gray area shows the uncertainty on the T-cube resistivity.

Combined with the reported amplitudes of the lattice specific heat, C_{ph} [26], and the sound velocity, v_{ph} [23], our data yields l_{ph} . The result is shown in figure 3d. At $T \approx 4$ K, $l_{ph} \simeq 4 \mu\text{m}$ well below the sample thickness (200 μm). Presumably, in CsV₃Sb₅, scattering of phonons by electrons impedes to reach the ballistic regime at above the superconducting transition.

Defining the electronic thermal resistivity as $WT = \frac{L_0 T}{\kappa_e}$ allows a quantitative comparison between the electronic heat transport and its charge counterpart. One expects the thermal resistivity to follow:

$$WT = WT_0 + B_2 T^2 + B_3 T^3 \quad (3)$$

The first term, WT_0 represents scattering by impurities and defects. The quadratic term is due to electron-electron scattering and finally, the cubic term is due to electron-phonon scattering. The validity of the WF law at $T=0$ imposes $WT_0 = \rho_0$. Its invalidity at finite temperature implies that $B_2 \neq A_2$. In

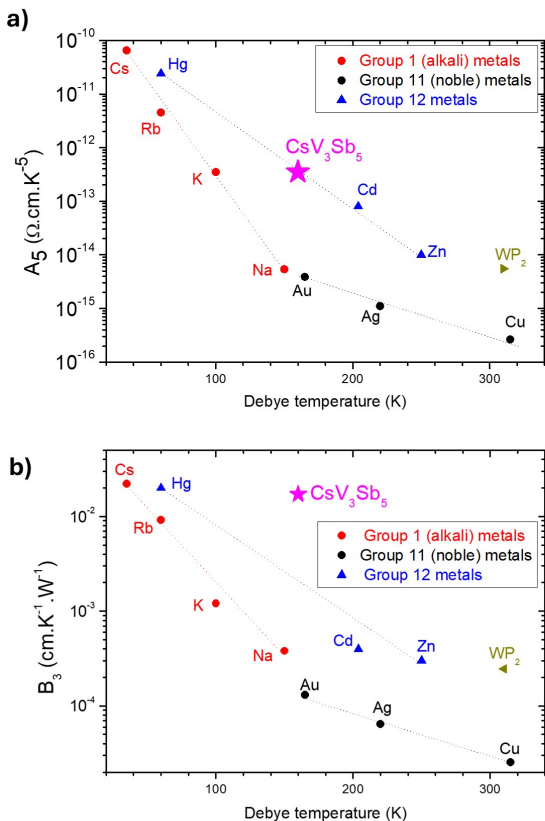


Figure 5: a) Amplitude of the prefactor of T^5 resistivity in CsV_3Sb_5 and in several elemental metals as a function of Debye temperature. Dashed lines indicate correlation between metals belonging to the same column of the periodic table. b) Same for the prefactor of thermal resistivity (expressed in its original units of $\text{cm.K}^{-1}.\text{W}^{-1}$ and without multiplication by L_0 .) The main source of listed values for elements are two tables in ref.[49]. The amplitude of B_3 in gold is misprinted and the correct value is recovered by referring to data reported in ref. [50]. We used ref. [51, 52] for A_5 values of column 12 elements. Dotted lines are guides for eye connecting metals belonging to the same group. The figure indicates that, considering its Debye temperature, CsV_3Sb_5 has relatively large e-ph prefactors.

the case of electron-phonon scattering, even the exponent changes. In thermal transport, it is $\propto T^3$, because only the variation of the phonon population matters. In electric transport, it is $\propto T^5$, because not all phonons matter equally. Note that the prefactor of T^5 electric resistivity and the prefactor of T^3 thermal resistivity both scale inversely with the Debye temperature, but also with the specific material-dependent parameters, which set the strength of e-ph coupling in a given metal [53].

Figures 4a-b compare our data with what is expected by Equation 3. Figure 4a is a plot of WT as a function of T^2 . In the lowest temperature range, WT is a linear in T^2 with an intercept, which yields $WT_0 = \rho_0$. The slope is significantly larger than the slope of electric resistivity. Above 8 K, there is an upward deviation

pointing to the emergence of a higher exponent. Plotting $WT - WT_0 + B_2T^2$ as a function of T^3 in Fig. 4b, allows to identify a cubic regime below ≈ 20 K.

The amplitude of B_2 , extracted by a quadratic fit to WT yields $B_2 = 6.6 \pm 0.9 \text{ n}\Omega.\text{cm.K}^{-2}$. The B_2/A_2 ratio in CsV_3Sb_5 is 5.2. This ratio, which is found to exceed unity in all explored cases, ranges between 1.6 and 7 (See table S1 in the supplement). Our result, by putting CsV_3Sb_5 in the upper part of this range, indicates that a large B_2/A_2 can be attained even in the absence of compensation, which was put theoretically proposed [54], as a possible driver of a large B_2/A_2 ratio, which was assumed to be forbidden by an early theoretical study [55].

We saw above that the remarkably large amplitude of A_5 points to a large collision cross section between electrons and phonons in CsV_3Sb_5 . This is confirmed in the thermal transport channel. The relative amplitude of B_3 , compared to other metals with a similar Debye temperature, is even larger.

Figure 5 compares the amplitude of A_5 and B_3 in CsV_3Sb_5 with a number of elemental metals. In each family, one can see a specific correlation between which A_5 and Θ_D . A similar (albeit less straightforward) family-dependent correlation between B_3 and Θ_D is also visible. Note that group 12 elements (Zn, Cd, Hg) with a HCP structure have a larger A_5 and B_3 than group 11 elements (Cu, Ag, Au) reflecting a larger electron-phonon cross section due to the proximity of the structural transition occurring between the two columns [56]. The absence of superconductivity in noble and alkali metals is often attributed to the weakness of e-ph coupling. Group 12 elements have superconducting ground states and known to have a larger e-ph coupling constant.

In absence of a systematic study of other members of AV_3Sb_5 , we can limit ourselves to a simple observation. The e-ph collision cross section in CsV_3Sb_5 , normalized to its Debye temperature is larger than these elemental metals. Note that this statement is about the CDW state. An estimation of the e-ph coupling constant from T-linear resistivity (see the supplement) finds that $\lambda \simeq 0.7$, in agreement with a previous study [57].

Thus, our results indicate that in CsV_3Sb_5 , the e-ph is significantly enhanced. This is consistent with what was previously found by studies employing neutron scattering [58], Raman spectroscopy [59] and angle-resolved photoemission spectroscopy [57]. We note that *Ab Initio* calculations [60] find a close competition between crystal structures with different symmetries to become the ground state of this solid. The consequences of this competition for e-ph collision rate emerges as a subject for future theoretical studies.

In summary, by measuring electrical and thermal conductivities of CsV_3Sb_5 , we separated the electronic

and the phononic contributions to heat transport. We found that the transport properties can be depicted in the standard picture of transport in metallic Fermi liquids. Comparison with other metallic Fermi liquids indicates that electrons suffer a moderate rate of collisions with other electrons and a strong one with phonons.

This work was supported by the Agence Nationale de la Recherche (ANR-25-CE30-5730-01) and by a grant attributed by the Ile de France regional council. SDW and ACS gratefully acknowledge support via the UC Santa Barbara NSF Quantum Foundry funded via the Q-AMASE-i program under award DMR-1906325.

-
- [1] B. R. Ortiz, L. C. Gomes, J. R. Morey, M. Winiarski, M. Bordelon, J. S. Mangum, I. W. Oswald, J. A. Rodriguez-Rivera, J. R. Neilson, S. D. Wilson, *et al.*, New kagome prototype materials: discovery of KV_3Sb_5 , RbV_3Sb_5 , and CsV_3Sb_5 , *Physical Review Materials* **3**, 094407 (2019).
- [2] B. R. Ortiz, S. M. Teicher, Y. Hu, J. L. Zuo, P. M. Sarte, E. C. Schueller, A. M. Abeykoon, M. J. Krogstad, S. Rosenkranz, R. Osborn, *et al.*, CsV_3Sb_5 : A z_2 topological kagome metal with a superconducting ground state, *Physical Review Letters* **125**, 247002 (2020).
- [3] S. D. Wilson and B. R. Ortiz, AV_3Sb_5 kagome superconductors, *Nature Reviews Materials* **9**, 420 (2024).
- [4] Y. Xu, Z. Ni, Y. Liu, B. R. Ortiz, Q. Deng, S. D. Wilson, B. Yan, L. Balents, and L. Wu, Three-state nematicity and magneto-optical kerr effect in the charge density waves in kagome superconductors, *Nature physics* **18**, 1470 (2022).
- [5] R. Khasanov, D. Das, R. Gupta, C. Mielke III, M. Elender, Q. Yin, Z. Tu, C. Gong, H. Lei, E. T. Ritz, *et al.*, Time-reversal symmetry broken by charge order in CsV_3Sb_5 , *Physical Review Research* **4**, 023244 (2022).
- [6] H. Gui, L. Yang, X. Wang, D. Chen, Z. Shi, J. Zhang, J. Wei, K. Zhou, W. Schnelle, Y. Zhang, *et al.*, Probing orbital magnetism of a kagome metal CsV_3Sb_5 by a tuning fork resonator, *Nature Communications* **16**, 1 (2025).
- [7] D. R. Saykin, C. Farhang, E. D. Kountz, D. Chen, B. R. Ortiz, C. Shekhar, C. Felser, S. D. Wilson, R. Thomale, J. Xia, *et al.*, High resolution polar kerr effect studies of CsV_3Sb_5 : Tests for time-reversal symmetry breaking below the charge-order transition, *Physical Review Letters* **131**, 016901 (2023).
- [8] C. Guo, G. Wagner, C. Putzke, D. Chen, K. Wang, L. Zhang, M. Gutierrez-Amigo, I. Errea, M. G. Vergniory, C. Felser, *et al.*, Correlated order at the tipping point in the kagome metal CsV_3Sb_5 , *Nature Physics* **20**, 579 (2024).
- [9] K. Jiang, T. Wu, J.-X. Yin, Z. Wang, M. Z. Hasan, S. D. Wilson, X. Chen, and J. Hu, Kagome superconductors AV_3Sb_5 ($a = k, rb, cs$), *National Science Review* **10**, nwac199 (2023).
- [10] T. Neupert, M. M. Denner, J.-X. Yin, R. Thomale, and M. Z. Hasan, Charge order and superconductivity in kagome materials, *Nature Physics* **18**, 137 (2022).
- [11] T. Park, M. Ye, and L. Balents, Electronic instabilities of kagome metals: saddle points and landau theory, *Physical Review B* **104**, 035142 (2021).
- [12] W. Liège, Y. Xie, D. Bounoua, Y. Sidis, F. Bourdarot, Y. Li, Z. Wang, J.-X. Yin, P. Dai, and P. Bourges, Search for orbital magnetism in the kagome superconductor CsV_3Sb_5 using neutron diffraction, *Physical Review B* **110**, 195109 (2024).
- [13] D. Chen, B. He, M. Yao, Y. Pan, H. Lin, W. Schnelle, Y. Sun, J. Gooth, L. Taillefer, and C. Felser, Anomalous thermoelectric effects and quantum oscillations in the kagome metal CsV_3Sb_5 , *Physical Review B* **105**, L201109 (2022).
- [14] X. Wei, C. Tian, H. Cui, Y. Zhai, Y. Li, S. Liu, Y. Song, Y. Feng, M. Huang, Z. Wang, *et al.*, Three-dimensional hidden phase probed by in-plane magnetotransport in kagome metal CsV_3Sb_5 thin flakes, *Nature Communications* **15**, 5038 (2024).
- [15] Q. Stahl, D. Chen, T. Ritschel, C. Shekhar, E. Sadrolahi, M. Rahn, O. Ivashko, M. v. Zimmermann, C. Felser, and J. Geck, Temperature-driven reorganization of electronic order in CsV_3Sb_5 , *Physical Review B* **105**, 195136 (2022).
- [16] L. Nie, K. Sun, W. Ma, D. Song, L. Zheng, Z. Liang, P. Wu, F. Yu, J. Li, M. Shan, *et al.*, Charge-density-wave-driven electronic nematicity in a kagome superconductor, *Nature* **604**, 59 (2022).
- [17] B. R. Ortiz, S. M. L. Teicher, L. Kautzsch, P. M. Sarte, N. Ratcliff, J. Harter, J. P. C. Ruff, R. Sheshadri, and S. D. Wilson, Fermi surface mapping and the nature of charge-density-wave order in the kagome superconductor csv_3sb_5 , *Phys. Rev. X* **11**, 041030 (2021).
- [18] X. Huang, C. Guo, C. Putzke, M. Gutierrez-Amigo, Y. Sun, M. G. Vergniory, I. Errea, D. Chen, C. Felser, and P. J. W. Moll, Three-dimensional fermi surfaces from charge order in layered CsV_3Sb_5 , *Phys. Rev. B* **106**, 064510 (2022).
- [19] K. Shrestha, R. Chapai, B. K. Pokharel, D. Miertschin, T. Nguyen, X. Zhou, D. Y. Chung, M. G. Kanatzidis, J. F. Mitchell, U. Welp, D. Popović, D. E. Graf, B. Lorenz, and W. K. Kwok, Nontrivial fermi surface topology of the kagome superconductor CsV_3Sb_5 probed by de haas-van alphen oscillations, *Phys. Rev. B* **105**, 024508 (2022).
- [20] C. Broyles, D. Graf, H. Yang, X. Dong, H. Gao, and S. Ran, Effect of the interlayer ordering on the fermi surface of kagome superconductor csv_3sb_5 revealed by quantum oscillations, *Phys. Rev. Lett.* **129**, 157001 (2022).
- [21] W. Zhang, L. Wang, C. W. Tsang, X. Liu, J. Xie, W. C. Yu, K. T. Lai, and S. K. Goh, Emergence of large quantum oscillation frequencies in thin flakes of the kagome superconductor csv_3sb_5 , *Phys. Rev. B* **106**, 195103 (2022).
- [22] W. Zhang, T. F. Poon, C. W. Tsang, W. Wang, X. Liu, J. Xie, S. T. Lam, S. Wang, K. T. Lai, A. Pourret, G. Seyfarth, G. Knebel, W. C. Yu, and S. K. Goh, Large fermi surface in pristine kagome metal CsV_3Sb_5 and enhanced quasiparticle effective masses, *Proceedings of the National Academy of Sciences* **121**, e2322270121 (2024).
- [23] Y. Pang, J. Liu, X. Fan, H. Yang, J. Zhu, Z. Wang, Y. Yao, X. Qian, and R. Yang, Glasslike cross-plane thermal conductivity of the kagome metals RbV_3Sb_5 and CsV_3Sb_5 , *Physical Review B* **108**, 205112 (2023).
- [24] E. D. Kountz, C. R. Murthy, D. Chen, L. Ye, M. P. Zic, C. Felser, I. R. Fisher, S. A. Kivelson, and A. Ka-

- pitulnik, Thermal transport measurements through the charge density wave transition in CsV₃Sb₅, *Physical Review B* **109**, L201120 (2024).
- [25] M. S. Hossain, Q. Zhang, E. S. Choi, D. Ratkovski, B. Lüscher, Y. Li, Y.-X. Jiang, M. Litskevich, Z.-J. Cheng, J.-X. Yin, *et al.*, Unconventional gapping behaviour in a kagome superconductor, *Nature Physics* , 1 (2025).
- [26] K. Yang, W. Xia, X. Mi, L. Zhang, Y. Gan, A. Wang, Y. Chai, X. Zhou, X. Yang, Y. Guo, *et al.*, Charge fluctuations above t cdw revealed by glasslike thermal transport in kagome metals AV₃Sb₅ (A= K, Rb, Cs), *Physical Review B* **107**, 184506 (2023).
- [27] A. Legros, S. Benhabib, W. Tabis, F. Laliberté, M. Dion, M. Lizaire, B. Vignolle, D. Vignolles, H. Raffy, Z. Z. Li, P. Auban-Senzier, N. Doiron-Leyraud, P. Fournier, D. Colson, L. Taillefer, and C. Proust, Universal t-linear resistivity and planckian dissipation in overdoped cuprates, *Nature Physics* **15**, 142 (2019).
- [28] J. Wang, L. Yang, C. W. Rischau, Z. Xu, Z. Ren, T. Lorenz, J. Hemberger, X. Lin, and K. Behnia, Charge transport in a polar metal, *npj Quantum Materials* **4**, 61 (2019).
- [29] M. J. Rice, Electron-electron scattering in transition metals, *Phys. Rev. Lett.* **20**, 1439 (1968).
- [30] K. Kadowaki and S. Woods, Universal relationship of the resistivity and specific heat in heavy-fermion compounds, *Solid State Communications* **58**, 507 (1986).
- [31] K. Behnia, On the origin and the amplitude of T-square resistivity in Fermi liquids, *Annalen der Physik* **534**, 2100588 (2022).
- [32] X. Lin, B. Fauqué, and K. Behnia, Scalable T^2 resistivity in a small single-component fermi surface, *Science* **349**, 945 (2015).
- [33] J. Wang, J. Wu, T. Wang, Z. Xu, J. Wu, W. Hu, Z. Ren, S. Liu, K. Behnia, and X. Lin, T-square resistivity without umklapp scattering in dilute metallic Bi₂O₂Se, *Nature Communications* **11**, 3846 (2020).
- [34] W. Duan, Z. Nie, S. Luo, F. Yu, B. R. Ortiz, L. Yin, H. Su, F. Du, A. Wang, Y. Chen, *et al.*, Nodeless superconductivity in the kagome metal CsV₃Sb₅, *Science China Physics, Mechanics & Astronomy* **64**, 107462 (2021).
- [35] R. A. Matula, Electrical resistivity of copper, gold, palladium, and silver, *Journal of Physical and Chemical Reference Data* **8**, 1147 (1979).
- [36] X. Zhou, H. Liu, W. Wu, K. Jiang, Y. Shi, Z. Li, Y. Sui, J. Hu, and J. Luo, Anomalous thermal hall effect and anomalous nernst effect of CsV₃Sb₅, *Physical Review B* **105**, 205104 (2022).
- [37] G. K. White and S. B. Woods, The thermal and electrical resistivity of bismuth and antimony at low temperatures, *The Philosophical Magazine: A Journal of Theoretical Experimental and Applied Physics* **3**, 342 (1958).
- [38] A. Jaoui, B. Fauqué, and K. Behnia, Thermal resistivity and hydrodynamics of the degenerate electron fluid in antimony, *Nature Communications* **12**, 195 (2021).
- [39] A. Jaoui, A. Gourgout, G. Seyfarth, A. Subedi, T. Lorenz, B. Fauqué, and K. Behnia, Formation of an electron-phonon bifluid in bulk antimony, *Phys. Rev. X* **12**, 031023 (2022).
- [40] A. Gourgout, A. Marguerite, B. Fauqué, and K. Behnia, Electronic thermal resistivity and quasi-particle collision cross section in semimetals, *Physical Review B* **110**, 155119 (2024).
- [41] W. Xie, F. Yang, L. Xu, X. Li, Z. Zhu, and K. Behnia, Purity-dependent Lorenz number, electron hydrodynamics and electron-phonon coupling in WTe₂, *Science China Physics, Mechanics & Astronomy* **67**, 287014 (2024).
- [42] S. Jiang, B. Fauqué, and K. Behnia, T-square dependence of the electronic thermal resistivity of metallic strontium titanate, *Physical Review Letters* **131**, 016301 (2023).
- [43] Y. Ling, F. Pawula, R. Daou, B. Fauqué, and K. Behnia, T-square electric resistivity and its thermal counterpart in RuO₂, *arXiv preprint arXiv:2511.04278* (2025).
- [44] J. Paglione, M. Tanatar, D. Hawthorn, R. Hill, F. Ronning, M. Sutherland, L. Taillefer, C. Petrovic, and P. Canfield, Heat transport as a probe of electron scattering by spin fluctuations: The case of antiferromagnetic CeRhIn₅, *Physical review letters* **94**, 216602 (2005).
- [45] B. Lussier, B. Ellman, and L. Taillefer, Anisotropy of heat conduction in the heavy fermion superconductor UPt₃, *Physical Review Letters* **73**, 3294 (1994).
- [46] D. K. Wagner, J. C. Garland, and R. Bowers, Low-temperature electrical and thermal resistivities of tungsten, *Phys. Rev. B* **3**, 3141 (1971).
- [47] A. Jaoui, B. Fauqué, C. W. Rischau, A. Subedi, C. Fu, J. Gooth, N. Kumar, V. Süß, D. L. Maslov, C. Felser, *et al.*, Departure from the Wiedemann–Franz law in WP₂ driven by mismatch in T-square resistivity prefactors, *npj Quantum Materials* **3**, 64 (2018).
- [48] C. Kittel and P. McEuen, *Introduction to solid state physics* (John Wiley & Sons, 2018).
- [49] P. G. Klemens, Thermal conductivity of solids at low temperatures, in *Low Temperature Physics I / Kältophysik I*, edited by S. Flügge (Springer Berlin Heidelberg, Berlin, Heidelberg, 1956) pp. 198–281.
- [50] G. K. White, The thermal conductivity of gold at low temperatures, *Proceedings of the Physical Society. Section A* **66**, 559 (1953).
- [51] P. D. Desai, T. K. Chu, H. M. James, and C. Y. Ho, Electrical resistivity of selected elements, *Journal of Physical and Chemical Reference Data* **13**, 1069 (1984).
- [52] E. Ryan, J. Jackson, and Y. Lwin, Resistivity of solid mercury, *Cryogenics* **20**, 158 (1980).
- [53] J. M. Ziman, *Electrons and phonons: the theory of transport phenomena in solids* (Oxford university press, 2001).
- [54] S. Li and D. L. Maslov, Lorentz ratio of a compensated metal, *Physical Review B* **98**, 245134 (2018).
- [55] C. Herring, Simple property of electron-electron collisions in transition metals, *Phys. Rev. Lett.* **19**, 167 (1967).
- [56] A. Subedi and K. Behnia, Deep-lying semi-dirac fermions in hexagonal close-packed cadmium, *Journal of Physics: Condensed Matter* **37**, 465501 (2025).
- [57] Y. Zhong, S. Li, H. Liu, Y. Dong, K. Aido, Y. Arai, H. Li, W. Zhang, Y. Shi, Z. Wang, S. Shin, H. N. Lee, H. Miao, T. Kondo, and K. Okazaki, Testing electron–phonon coupling for the superconductivity in kagome metal CsV₃Sb₅, *Nature Communications* **14**, 1945 (2023).
- [58] Y. Xie, Y. Li, P. Bourges, A. Ivanov, Z. Ye, J.-X. Yin, M. Z. Hasan, A. Luo, Y. Yao, Z. Wang, G. Xu, and P. Dai, Electron-phonon coupling in the charge density wave state of CsV₃Sb₅, *Phys. Rev. B* **105**,

- L140501 (2022).
- [59] G. He, L. Peis, E. F. Cuddy, Z. Zhao, D. Li, Y. Zhang, R. Stumberger, B. Moritz, H. Yang, H. Gao, T. P. Devereaux, and R. Hackl, Anharmonic strong-coupling effects at the origin of the charge density wave in CsV_3Sb_5 , *Nature Communications* **15**, 1895 (2024).
 - [60] A. Subedi, Hexagonal-to-base-centered-orthorhombic $4Q$ charge density wave order in kagome metals KV_3Sb_5 , RbV_3Sb_5 , and CsV_3Sb_5 , *Phys. Rev. Mater.* **6**, 015001 (2022).
 - [61] P. B. Allen, Empirical electron-phonon λ values from resistivity of cubic metallic elements, *Phys. Rev. B* **36**, 2920 (1987).
 - [62] C. Zhao, L. Wang, W. Xia, Q. Yin, H. Deng, G. Liu, J. Liu, X. Zhang, J. Ni, Y. Huang, *et al.*, Ultralow-temperature heat transport evidence for residual density of states in the superconducting state of CsV_3Sb_5 , *Chinese Physics Letters* **41**, 127303 (2024).
 - [63] D. Zhang, K.-W. Chen, G. Zheng, F. Yu, M. Shi, Y. Zhu, A. Chan, K. Jenkins, J. Ying, Z. Xiang, *et al.*, Large oscillatory thermal Hall effect in kagome metals, *Nature Communications* **15**, 6224 (2024).

Supplementary Materials for "Amplitude of electron-electron and electron-phonon scattering terms in thermal and electric resistivities of CsV₃Sb₅"

Superconducting transition and electric resistivity in a magnetic field.

Figure S1a displays electrical resistivity between 2 K and 5 K for small applied magnetic field such that superconducting transition is visible. At zero magnetic field, the superconducting transition starts at 4.25 K. Figure S1b shows the residual resistivity (ρ_0) as a function of magnetic field. ρ_0 increases roughly linearly with magnetic field.

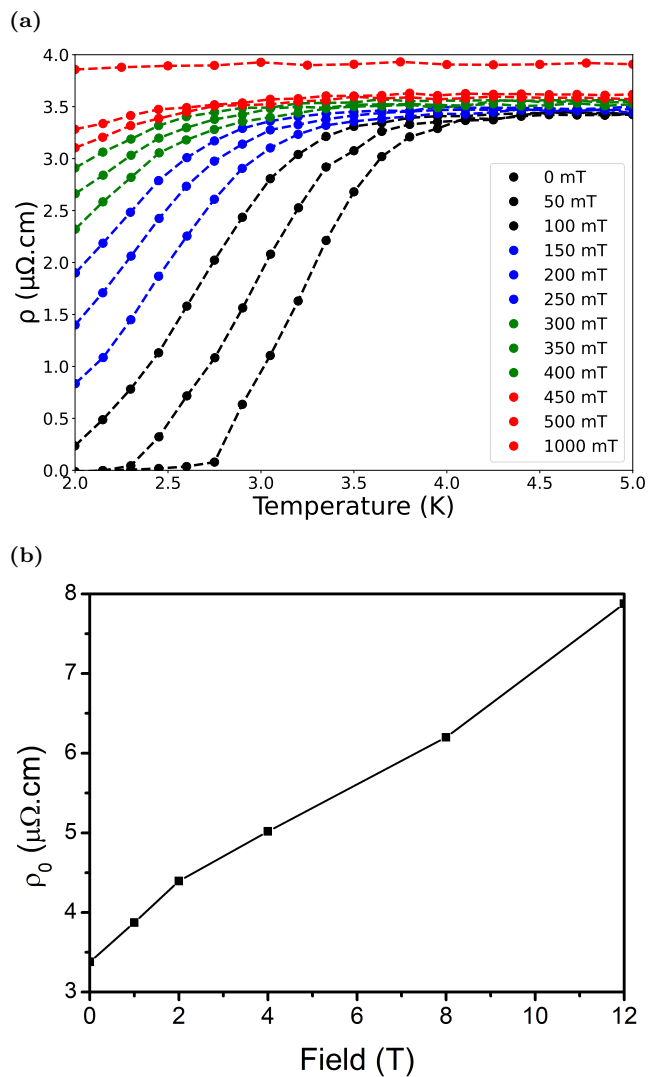


Figure S1: (a) In-plane resistivity of CsV₃Sb₅ between 2 K and 5 K with applied magnetic field up to 1 T. (b) Residual resistivity as function of magnetic field.

High-temperature electrical resistivity and e-ph coupling

Figure S2 is a plot of the in-plane resistivity (ρ_{xx}) of CsV₃Sb₅ from 2 K to 294 K. The resistivity becomes linear in temperature when $T \geq 200\text{K}$. with an estimated slope of $\frac{d\rho}{dT} \simeq 0.25 \mu\Omega\cdot\text{cm} \cdot \text{K}^{-1}$.

According to the Bloch–Grüneisen picture of electron–phonon scattering, the resistivity becomes T-linear once T is comparable to or larger than the Debye temperature θ_D . In this limit [61]:

$$\frac{d\rho}{dT} = 2\pi\lambda k_B \frac{\hbar}{e^2} \frac{n}{m^*} \quad (\text{S1})$$

Here, λ is the electron–phonon coupling constant, n the carrier density and m^* the effective mass of the carriers. Above the CDW phase, the Fermi surface is formed by two large bands. According to quantum oscillation studies under pressure [22], the largest band, labeled ζ , has a frequency of $F_\zeta = 8.16 \text{ kT}$, an effective mass of $m^* = 1.6m_0$, and a two-dimensional character. For this quasi-2D band, we estimate the carrier density to be $n \simeq 1.3 \times 10^{22} \text{ cm}^{-3}$, which leads to $\lambda = 0.7$, comparable to the intermediate value $\lambda = 0.45\text{--}0.6$ estimated by laser-based angle-resolved photoemission spectroscopy [57].

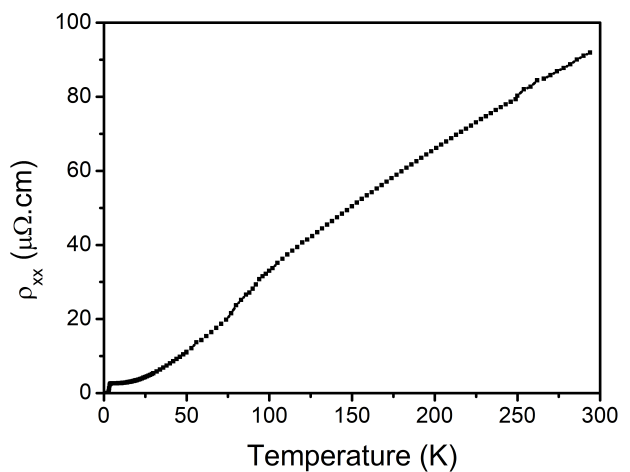


Figure S2: In plane resistivity of CsV₃Sb₅ as function of temperature.

A comparison with previously reported data

Thermal transport in CsV₃Sb₅ has been studied by several groups [24–26, 36, 62, 63].

As seen in Fig. S3, when the temperature range of interest overlaps, there is a significant discrepancy between some sets of data. One can see that between 2 K and 10 K, our data is in agreement with what was reported by two other groups, but almost 8 times lower than what was reported by another. Moreover, at 30 K, there is a significant discrepancy between

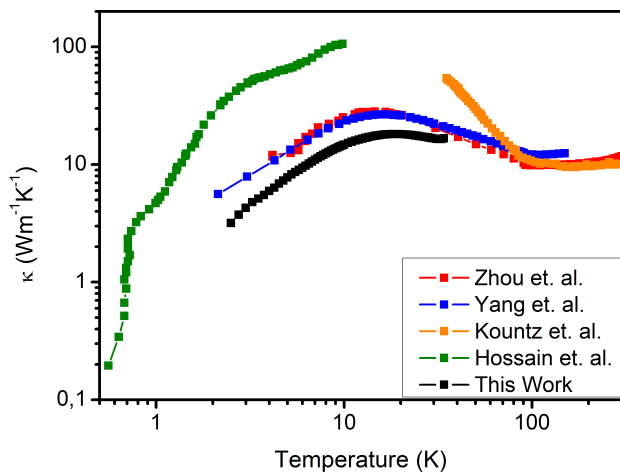


Figure S3: Zero-field thermal conductivity of CsV_3Sb_5 reported by different groups [24–26, 36]. A large scattering is observed between five sets of data. Our data appears to agree with what was reported by Zhou *et al.* [36] and by Yang *et al.* [26]. There is a significant difference between these three data sets and what was reported by Hossain *et al.* [25] and by Kountz *et al.* [24].

what is reported by these two groups and what was reported by another group. However, this discrepancy vanishes at 100 K, that is above the CDW transition temperature.

All groups used an identical method. However, they did not systemically report on the verification of their thermal transport data by recovering the Wiedemann-Franz law in the zero-temperature limit. Nevertheless, it is unlikely that this discrepancy is due to a measurement error. A more interesting possibility is that small differences between single crystalline samples drastically affects the increase in the thermal conductivity induced by the CDW transition. This hypothesis is to be tested by future studies covering the whole temperature range.

At this stage, it is fair to make a few qualitative remarks. Two different kinds of behavior are visible in Fig. S3. Three sets of data almost overlap. This is the case of present study and those reported by Zhou *et al.* [36] and by Yang *et al.* [26]). On the other hand, and in contrast with this consistency, the data reported by Hossain *et al.* [25] and restricted to below 10K, is almost five times larger. Kountz *et al.* [24] also report a thermal conductivity three times larger than the data reported by Zhou *et al.* [36] and Yang *et al.* [26] between 40 K and 80 K. Because of the difference in the temperature ranges explored, the consistency between [25] and [24] can only be guessed. Since the remarkably large thermal

resistivity driven by e-ph coupling is expected to be strain-dependent, the presence of uncontrolled strain is a plausible source of this sample dependence.

Thermal conductivity at magnetic fields exceeding 1T

Figure S4a plots estimated L_e/L_0 using the difference in conductivities between 0 T and 1 T (black) or 0 T and 12 T (red). In both cases, L_e/L_0 tends to zero below 4 K due to the apparition of superconductivity, in this case Wiedemann-Franz law does not apply. For temperatures above 4 K, difference between 0 T and 12 T yields to a higher L_e compares to the other case. In particular, L_e/L_0 seems to tend to 1.2 at low temperature. This overall increase of L_e is not only restricted to conductivities at 12 T but is also observed when we subtracted conductivity between 0 T and any field above 1 T. This indicates that when the magnetic field when exceeds 1 T, either L_e or the phonon thermal conduction are significantly affected by the magnetic field field.

Figure S4b plots the difference between zero-field and finite-field thermal and electric conductivities, at 20 K. For all magnetic fields, the difference in electrical conductivity is larger than its thermal counterpart, confirming that $L_e/L_0 < 1$. A kink between 0 T and 1 T is visible in the field dependence of thermal conductivity, but not in the the field dependence of electric conductivity. Clarifying the origin of this field-induced change in thermal transport is a task for future studies.

The T-square electric and thermal resistivity prefactors

Table S1 lists a selection of reported amplitudes of A_2 and B_2 , the prefactors of T-square electric and thermal resistivities. Both are expressed in units of $\text{n}\Omega\cdot\text{cm}\cdot\text{K}^{-2}$. In all cases, $B_2/A_2 > 1$. CsV_3Sb_5 does not differ from other cases. Taken at its face value, this remarkably large B_2/A_2 indicates that, in this solid, a large fraction of e-e scattering is either small angle or Normal (i.e. not Umklapp).

The differentiation between “vertical” and “horizontal” scattering events pulls down the prefactor for electrical resistivity. Herring [55] argued that this difference is bounded an therefore the B_2/A_2 cannot exceed 2. Li and Maslov [54] argued that in a compensated semimetal this boundary can be exceeded. The fact that CsV_3Sb_5 is not a compensated metal implies that compensation is not a necessary condition for $B_2/A_2 > 2$.

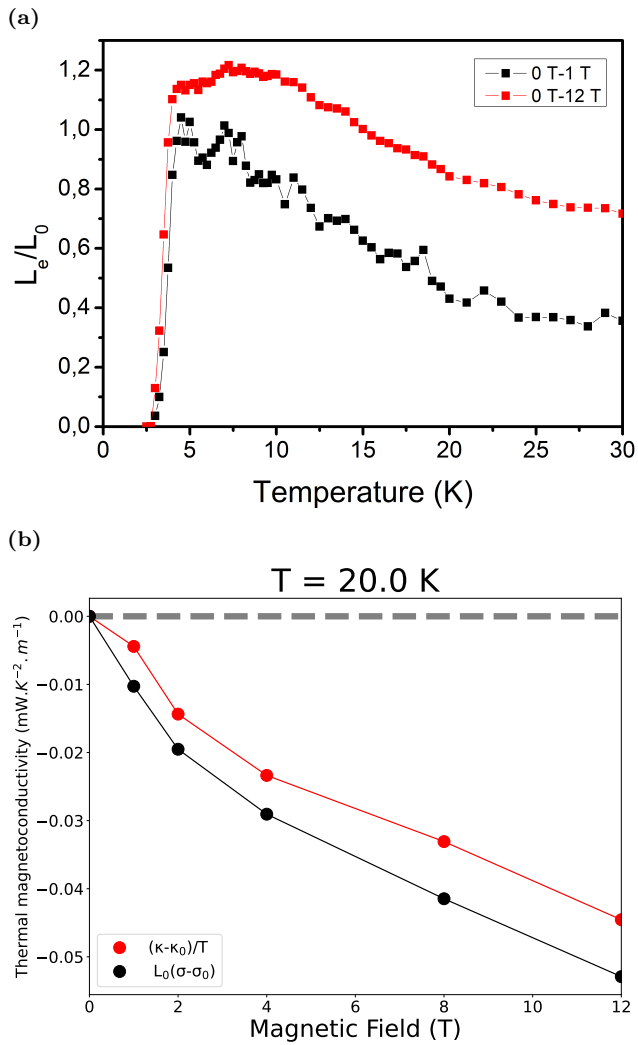


Figure S4: (a) L_e/L_0 calculated from the difference in conductivities between 0 T and 1 T or 0 T and 12 T. (b) Difference of conductivities between zero magnetic field (σ_0 and κ_0) and finite, at 20 K.

Material	A_2	B_2	B_2/A_2	Ref.
W	8.7×10^{-4}	6×10^{-3}	6.9	[46]
Bi	12	35	2.9	[40]
Sb	0.3	0.6	2.0	[38]
WTe ₂	4.5	11	2.4	[41]
WP ₂	0.017	0.074	4.6	[47]
CeRhIn ₅	21	57	2.7	[44]
RuO ₂	0.071	0.26	3.7	[43]
CsV ₃ Sb ₅	1.26	6.6	5.2	This work

Table S1: Reported values of electric and thermal T-square prefactors.